Journal of Solid State Chemistry 181 (2008) 1321–1329

Contents lists available at ScienceDirect

Journal of Solid State Chemistry

journal homepage: www.elsevier.com/locate/jssc

# Structural and electrical properties of the $2Bi_2O_3 \cdot 3ZrO_2$ system

Čedomir Jovalekić [a], Miodrag Zdujić [b,*], Dejan Poleti [c], Ljiljana Karanović [d], Miodrag Mitrić [e]

[a] Institute for Multidisciplinary Research, Kneza Višeslava 1, 11000 Belgrade, Serbia
[b] Institute of Technical Sciences of the Serbian Academy of Sciences and Arts, Knez Mihailova 35, 11000 Belgrade, Serbia
[c] Department of General and Inorganic Chemistry, Faculty of Technology and Metallurgy, Karnegijieva 4, 11000 Belgrade, Serbia
[d] Laboratory of Crystallography, Faculty of Mining and Geology, Đušina 7, 11000 Belgrade, Serbia
[e] Laboratory of Solid State Physics, Institute for Nuclear Sciences "Vinča", P.O. Box 522, 11000 Belgrade, Serbia

ARTICLE INFO

*Article history:*
Received 10 September 2007
Received in revised form
19 February 2008
Accepted 28 February 2008
Available online 14 March 2008

*Keywords:*
Ferroelectricity
Mechanochemical treatment
$Bi_2O_3$
$ZrO_2$

ABSTRACT

Powder mixtures of $\alpha$-$Bi_2O_3$ (bismite) and monoclinic m-$ZrO_2$ (baddeleyite) in the molar ratio 2:3 were mechanochemically and thermally treated with the goal to examine the phases, which may appear during such procedures. The prepared samples were characterized by X-ray powder diffraction, differential scanning calorimetry (DSC), electrical measurements, as well as scanning electron microscopy (SEM) and transmission electron microscopy (TEM). The mechanochemical reaction leads to the gradual formation of a nanocrystalline phase, which resembles $\delta$-$Bi_2O_3$, a high-temperature $Bi_2O_3$ polymorph. Isothermal sintering in air at a temperature of 820 °C for 24 h followed by quenching to room temperature yielded a mixture of $ZrO_2$-stabilized $\beta$-$Bi_2O_3$ and m-$ZrO_2$ phases, whereas in slowly cooled products, the complete separation of the initial $\alpha$-$Bi_2O_3$ and m-$ZrO_2$ constituents was observed. The dielectric permittivity of the sintered samples significantly depended on the temperature. The sintered and quenched samples exhibited a hysteresis dependence of the dielectric shift, showing that the $ZrO_2$-doped $\beta$-$Bi_2O_3$ phase possess ferroelectric properties, which were detected for the first time. This fact, together with Rietveld refinement of the $\beta$-$Bi_2O_3$/m-$ZrO_2$ mixture based on neutron powder diffraction data showed that $ZrO_2$-doped $\beta$-$Bi_2O_3$ has a non-centrosymmetric structure with $P\bar{4}2_1c$ as the true space group. The $ZrO_2$ content in the doped $\beta$-$Bi_2O_3$ and the crystal chemical reasons for the stabilization of the $\beta$-$Bi_2O_3$ phase by the addition of m-$ZrO_2$ are discussed.



## 1. Introduction

Pure or doped $\delta$-$Bi_2O_3$ is the best high-temperature ionic conductor known [1–3]. At the same time, when doped with some lower valence cations (e.g., $Ca^{2+}$, $Sc^{3+}$, $Y^{3+}$, or rare-earth ions) $ZrO_2$ also shows a high oxide ion conductivity [3–5]. Both facts indicate the potential application of these materials as gas sensors and electrodes for solid oxide fuel cells [6]. On the other hand, a great interest for the synthesis and study of ferroelectric materials has arisen in the last two decades. Among these materials, some layered Bi compounds such as $Bi_4Ti_3O_{12}$, with a perovskite-type structure are of particular interest, because of their notable usage for the production of electronic components [7]. However, to the best of our knowledge the $Bi_4Zr_3O_{12}$ phase, analogous to $Bi_4Ti_3O_{12}$, has never been reported, although the geometric factor of stability (Goldsmith factor of tolerance) indicates a ferroelectric character of this hypothetical phase [8].

Thus, it appears that there are many reasons for studying the $Bi_2O_3$–$ZrO_2$ system in detail. This system was for the first time examined by Aurivillius and Sillen during their studies on body-centered cubic $\gamma$-$Bi_2O_3$ polymorphs stabilized with different cations. In the case of $Zr^{4+}$, a $\gamma$-$Bi_2O_3$ phase with a lattice parameter of 10.21 Å was reported [9].

While investigating the effect of the addition of various oxides on the corresponding $Bi_2O_3$ quasi-binary phase diagrams and stability of $Bi_2O_3$ polymorphs, Levin and Roth [10] described a high-temperature $\delta$-$Bi_2O_3$ solid solution with a cubic, fluorite-like structure in the $Bi_2O_3$–$ZrO_2$ system containing up to 28 mol% of $ZrO_2$. On heating, this solid solution appears at 710 °C and partially melts above 860 °C. The appearance of solid solutions with a tetragonal $\beta$-$Bi_2O_3$ structure when a mixture of $ZrO_2$ and the liquid phase was cooled below 860 °C was also reported.

Somewhat earlier, Hund [11] asserted the existence of a $\beta$-$Bi_2O_3$ solid solution for $Bi_2O_3$–$ZrO_2$ mixtures containing up to 82 mol% of $ZrO_2$. The products were easily prepared by heating at 800 °C for 0.5 h, but the post-thermal treatment (quenching or slow cooling) was not specified.

While investigating the $Bi_2O_3$–$ZrO_2$ and $Bi_2O_3$–$HfO_2$ systems, Sorokina and Slight [12] did not find such a high $ZrO_2$ solubility.

* Corresponding author. Fax: +381 11 2185 263.
*E-mail address:* zdujic@itn.sanu.ac.yu (M. Zdujić).

0022-4596/$ - see front matter © 2008 Elsevier Inc. All rights reserved.
doi:10.1016/j.jssc.2008.02.038

Instead, after heating at 600 °C, a $\delta$-$Bi_2O_3$ phase with the general formula $Bi_xZr_{1-x}O_{2-x/2}$ with $x \approx 0.5$–$0.75$ was obtained. However, the samples calcinated at 750 °C or at higher temperatures showed no $Bi_xZr_{1-x}O_{2-x/2}$ phase, but only a mixture of $Bi_{1.84}Zr_{0.16}O_{3.08}$, with $\beta$-$Bi_2O_3$ structure and m-$ZrO_2$ (baddeleyite) phases was obtained [12]. Once more, it is not clear whether the samples were quenched or slowly cooled.

Somewhat later, Abrahams et al. [13] came to a similar conclusion: in the $Bi_2O_3$–$ZrO_2$ system, the formation of $Bi_{2-x}Zr_xO_{3+x/2}$ ($0.05 < x < 0.17$) occurs when the corresponding oxide mixtures are quenched a-fter heating at 850 °C for 12 h.

The composition $Bi_{1.85}Zr_{0.15}O_{3.075}$ prepared by Abrahams et al. was further structurally characterized and refined in the tetragonal system, space group $P4_2/nmc$, using a combination of X-ray and neutron powder diffraction data [13]. Since the structure of $Bi_{1.85}Zr_{0.15}O_{3.075}$ is similar to that of $\beta$-$Bi_2O_3$, the new phase was termed as the $\beta_{III}$-phase. The main structural features of $Bi_{1.85}Zr_{0.15}O_{3.075}$ are the partial substitution of $Bi^{3+}$ for $Zr^{4+}$ and the existence of a new O3 atom, which is situated in $Bi_4O_4$ channels and involved in the heptacoordination of Zr. Both the Zr and O3 sites are of rather low (0.075) occupancy.

Very recently, an increase of the Zr content up to $x = 0.67$ in quenched $Bi_{2-x}Zr_xO_{3+\delta}$ with the $\beta_{III}$-$Bi_2O_3$ structure was reported again [14]. The increase of $x$ was attributed to the use of $ZrO(NO_3)_2$, instead of the usual $ZrO_2$ as the reactant in the solid-state reaction with $Bi_2O_3$.

From the foregoing, it appears that there are considerable discrepancies regarding the compounds or solid solutions and their stability, particularly in the region with higher $ZrO_2$ contents.

In this study, we focused on the $Bi_2O_3$–$ZrO_2$ system with 60 mol% of $ZnO_2$, i.e., the $2Bi_2O_3 \cdot 3ZrO_2$ composition, which is close to the upper limits of solubility reported by Hund [11] and Meatza et al. [14]. Besides, this composition corresponds to the above-mentioned ferroelectric $Bi_4Ti_3O_{12}$ phase. With the goal of investigate the phases which may be formed in this system, the $2Bi_2O_3 \cdot 3ZrO_2$ mixture was treated in two different ways. One was the thermal treatment followed by either quenching or slow (furnace) cooling. The other was mechanochemical treatment as a very convenient technique for producing metastable phases and (supersaturated) solid solutions, which are occasionally used as prepared or they can be further treated in order to tune their properties [15–17]. As related examples, such a treatment was applied for the preparation of doped $\gamma$-$Bi_2O_3$ phases [18], or the $TiO_2$ stabilized, high-temperature, cubic $ZrO_2$ phase [19].

Recently, the mechanochemical treatment of a $2Bi_2O_3 \cdot 3ZrO_2$ powder mixture using steel vials and balls as the milling medium was reported [8]. However, iron contamination, originating from the vial and balls debris, accumulated throughout the treatment, reaching a value of 13 at% Fe after 20 h of milling. As a result, Fe was found to participate in the mechanochemical reaction and subsequent reactive sintering. On account of this, it was decided to perform the milling of the $2Bi_2O_3 \cdot 3ZrO_2$ mixture in zirconia vials with zirconia balls.

## 2. Experimental procedure

A mixture of commercial $Bi_2O_3$ and $ZrO_2$ powders (both of >99% purity) in a 2:3 molar ratio was used as the starting material. By the X-ray powder diffraction (XPD) technique, $Bi_2O_3$ was identified as being in the $\alpha$-$Bi_2O_3$ (bismite) form, while $ZrO_2$ was mainly in the monoclinic (baddeleyite, denoted as m-$ZrO_2$) modification, but contained about 5 wt% of the high-temperature tetragonal polymorph (JCPDS card 42-1164).

Mechanochemical treatment was carried out in a Fritsch Pulverisette 5 planetary ball mill. Zirconia vials of 500 $cm^3$ charged with 93 zirconia balls of a nominal diameter of 10 mm were used as the milling medium. The mass of the powder mixture was 15 g, giving a ball-to-powder mass ratio of 20:1. The angular velocity of the supporting disk and vials was 33.2 (317) and 41.5 rad $s^{-1}$ (396 rpm), respectively. The mixtures were milled for 10 and 30 min, as well as 1, 2, 5, 10, 15, 20, and 50 h in an air atmosphere. Each milling run was carried out with a fresh powder mixture and without opening the vial.

The homogenized powder mixture (milling time 0 h), as well as the powders mechanochemically treated for various milling times were cold pressed (500 MPa) into pellets of 10 mm diameter and a thickness of about 1.5 mm, then isothermally sintered in air at 820 °C for 24 h and quenched in air to room temperature. For comparison, some milled samples were also furnace cooled after sintering.

An additional sample was also prepared from the initial powder mixture by heating (up to 780 °C; heating rate: 20 °C $min^{-1}$) and quenching. The chemical composition of this sample was analyzed quantitatively in eight points using a LINK AN 1000 EDS microanalyzer attached to a JEOL JSM-6460 LV Scanning Electron Microscope. The software ZAF-4/FLS provided by LINK was used for corrections. Metallic Zr and Bi were applied as standards.

Transmission electron microscopy (TEM) and selected area electron diffraction (SAED) analyses of the sample milled for 50 h were performed on a Philips M400 instrument.

The XPD data were collected on a Rigaku PH 1050 diffractometer with Cu$K\alpha$ graphite-monochromatized radiation ($\lambda = 0.15418$ nm) in the range 10–100° $2\theta$ (step length: 0.02° $2\theta$, scan time: 5 s). The program PowderCell [20] was used for preliminary phase analysis.

The sample mechanochemically treated for 1 h, isothermally sintered at 820 °C for 20 h and quenched was chosen for detailed structural characterization by the Rietveld method. For this sample, XPD data were collected as described above, but with a scan time of 18 s.

The neutron diffraction experiments were performed at the Swedish research reactor R2 in Studsvik. The data were collected at 295 and 10 ($\pm$1) K. The monochromatic neutron beam was obtained by a double monochromator system, using reflections from the (220) planes of two copper crystals, giving a wavelength of 1.474(1) Å. After collimation of $\alpha_1 = 12'$ and $\alpha_2 = 10'$, the neutron flux at the specimen was approximately $10^6$ $cm^{-2}$ $s^{-1}$. The powdered sample (a volume of about 3 $cm^3$) was placed in an 11 mm diameter vanadium tube. For the data collection, a computer controlled multidetector system with 35 separate detectors was used. The detectors scanned over range 4.00–135.92° $2\theta$ with a step length of 0.08°.

The Rietveld refinements of both, X-ray and neutron powder diffraction data were performed using the program FULLPROF [21] in the WinPLOTR environment [22]. The peak profiles were described by a pseudo-Voigt (X-ray diffraction) or Gaussian (neutron diffraction) function, whereas the Fourier filtering method with the window in the range 500–1500 points was used for the background description. Scattering factors for the neutral atoms were applied for the X-ray refinements.

Three structural models were tested assuming a mixture of m-$ZrO_2$ with (a) $Bi_{1.85}Zr_{0.15}O_{3.075}$ in the space group $P4_2/nmc$, (b) $Bi_{1.85}Zr_{0.15}O_{3.075}$ in the space group $P\bar{4}2_1c$, and (c) $\beta$-$Bi_2O_3$ in the space group $P\bar{4}2_1c$. For (a) and (b), the structural parameters published by Abrahams et al. [13] were used as the starting model (henceforth called the Abrahams model). The positions of Zr and O3 atoms and their displacement parameters were not refined, because of their rather low occupancy. For (c), the revised model

of the $\beta$-$Bi_2O_3$ phase described by Blower and Greaves [23] was used. The structural parameters given by Winterer et al. [24] were used as the starting values for the refinement of m-$ZrO_2$.

The thermal behavior of the initial mixture (milling time 0 h), powders milled for 30 min, 10, 20, and 50 h, as well as corresponding sintered and quenched samples was investigated from room temperature to 1000 °C using an SDT Q600 simultaneous differential scanning calorimetry DSC–TGA instrument (TA Instruments) with a heating and cooling rate of 20 K $min^{-1}$ under a dynamic (100 $cm^3$ $min^{-1}$) $N_2$ atmosphere.

Electrodes for the electrical measurements were applied to polished surfaces of the sintered disks by the screen-printing method. The silver paste was polymerized at 450 °C for 30 min. The capacitance was measured at a frequency of 1 and 10 kHz in the temperature range from room temperature to 750 °C using an LCZ impedance analyzer (Hewlett-Packard 4192A). The relative dielectric permittivity was calculated from the capacitance data by the relation $\varepsilon = Cd/\varepsilon_0 S$, where $C$ is the capacity, $d$ the thickness of the sample, $S$ the electrode area and $\varepsilon_0$ the permittivity of the free space ($8.85 \times 10^{-12}$ F $m^{-1}$). A standard Sawyer–Tower circuit was used for the hysteresis measurements (room temperature, electric field of 13.5 kV $cm^{-1}$). The unpoled samples were kept in a silicon oil bath to avoid air breakdown at high electric fields.

## 3. Results and discussion

### 3.1. Mechanochemical and thermal treatment

The XPD patterns of the initial mixture (milling time 0 h) and powders milled for various milling times are given in Fig. 1. Significant structural changes were observed already after 10 min of milling, and they were very pronounced for milling times up to 30 min, when the system passed through the state of minimum crystallinity. In this period, the peaks of both $\alpha$-$Bi_2O_3$ and m-$ZrO_2$ notably decreased and broadened as a result of crystallite size reduction and the introduction of lattice strain. After that it seems that a new phase appeared. The maxima of this new phase increased up to 2 h of milling (Fig. 1). With prolonged milling times, the structural changes were much slower but notable, indicating that deformational mixing progressed.

In the sample milled for 50 h, the average crystallite size, calculated by the Scherrer formula (with a highly crystalline $\alpha$-$Bi_2O_3$ as the standard) was 4 nm. On the other hand, the microstructure, as indicated by TEM (Fig. 2), consisted of very fine grains of about 8–10 nm immersed in an amorphous-like matrix. However, SAED did not confirm a significant presence of amorphous phase.

The peak broadening and the similarity of the $\beta$-$Bi_2O_3$ and $\delta$-$Bi_2O_3$ XPD patterns [25] preclude a straightforward interpretation of the XPD results for samples milled between 2 and 50 h. Therefore, an unambiguous phase assignment ($\beta$-$Bi_2O_3$ or $\delta$-$Bi_2O_3$) definitely required the supporting evidence (see later).

The phase composition of milled and sintered products is sensitive to the cooling rate, i.e., quenching versus slow (furnace) cooling, after the isothermal heat treatment. In the latter case, the products obtained at 820 °C always decomposed to the initial $\alpha$-$Bi_2O_3$ and m-$ZrO_2$ phases (Fig. 3).

The XPD analysis of all sintered and quenched samples revealed the identical phase composition regardless of the precursor used, i.e., the powders mechanochemically treated for various milling times. In fact, as already stated, the same phase composition was obtained after a continuous heating up to 780 °C and quenching of the initial powder mixture. The density of either the quenched or slowly cooled samples practically did not depend on the milling time. The measured sintered densities for quenched and slowly cooled samples were about 7.60 and 7.45 g $cm^{-3}$, respectively, meaning that 91–93% of the estimated theoretical density was achieved.

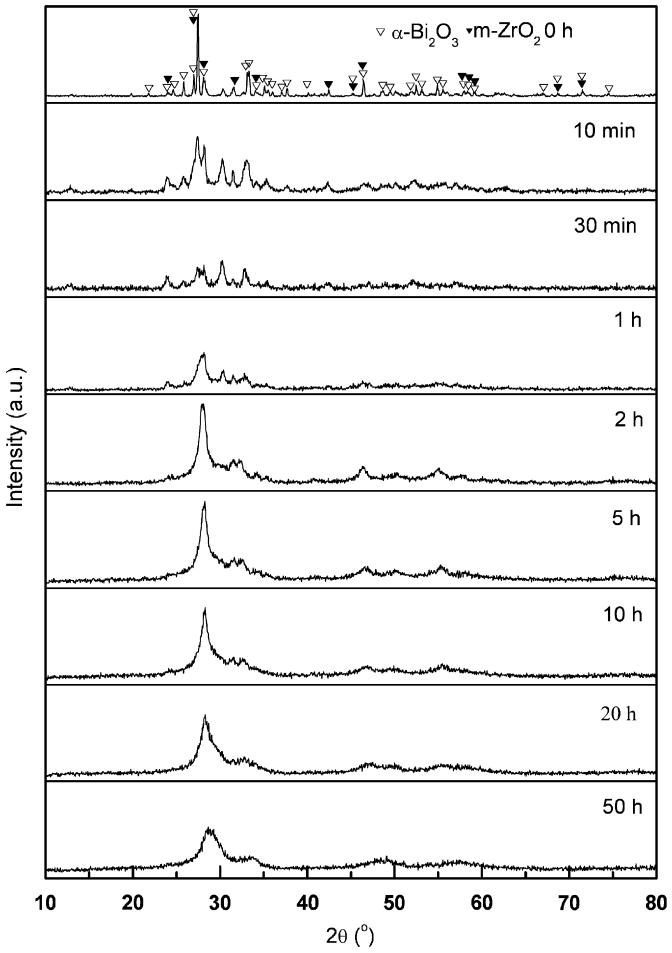


**Fig. 1.** XPD patterns of the $2Bi_2O_3 \cdot 3ZrO_2$ powder mixtures mechanochemically treated for various milling times.

At first sight, the routine XPD patterns of the quenched samples are easily indexed on the $\beta$- or $\beta_{III}$-$Bi_2O_3$ phase [13]. Only several very weak maxima that could be attributed to minor impurities remain unindexed. However, a more careful examination of the XPD data showed a high-angle shoulder at the most intense maximum and an anomalous width of the 0 0 2 maximum at 31.65° 2$\theta$ (Fig. 3a). This allowed the confirmation of the presence of another phase, which was further identified as m-$ZrO_2$ in an approximate amount of 30 wt% (the initial mixture contained 28.4 wt% of $ZrO_2$).

### 3.2. Thermal behavior

In the first heating, remarkably different DSC traces were obtained for the initial powder mixture, the sintered and quenched sample, and the powders mechanochemically treated for various milling times (Fig. 4). However, very similar thermal behaviors were obtained in the subsequent heat treatments, i.e., cooling and second heating, implying that the structure attained at 1000 °C is the same regardless of the starting state.

The DSC curve (first heating) of the initial mixture (Fig. 4a) shows a well-defined sharp endothermic peak at 731 °C (onset temperature) with an enthalpy of 61.41 J $g^{-1}$, which may be attributed to the $\alpha$-$\rightarrow\delta$-$Bi_2O_3$ phase transition. The obtained values for the temperature and molar enthalpy ($\Delta_m H = 28.6$ kJ $mol^{-1}$) are very similar to the literature values for the $\alpha \rightarrow \delta$ transition given by

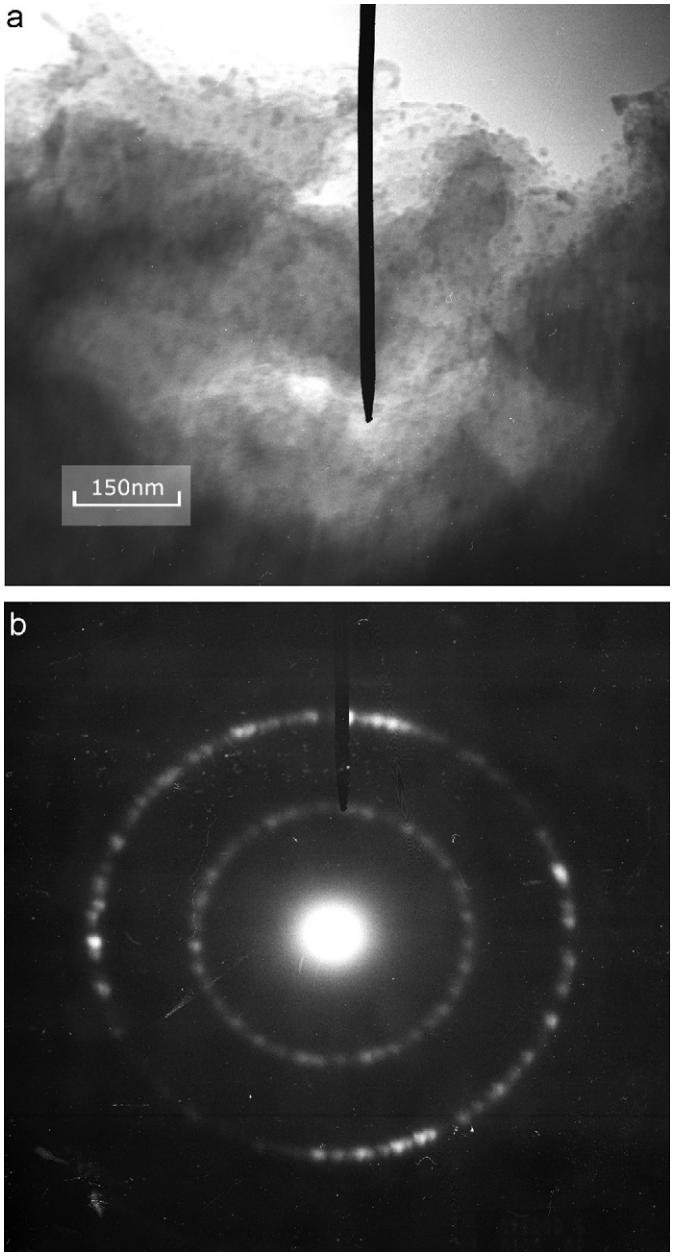


**Fig. 2.** TEM (a) and SAED (b) analysis of the sample milled for 50 h.

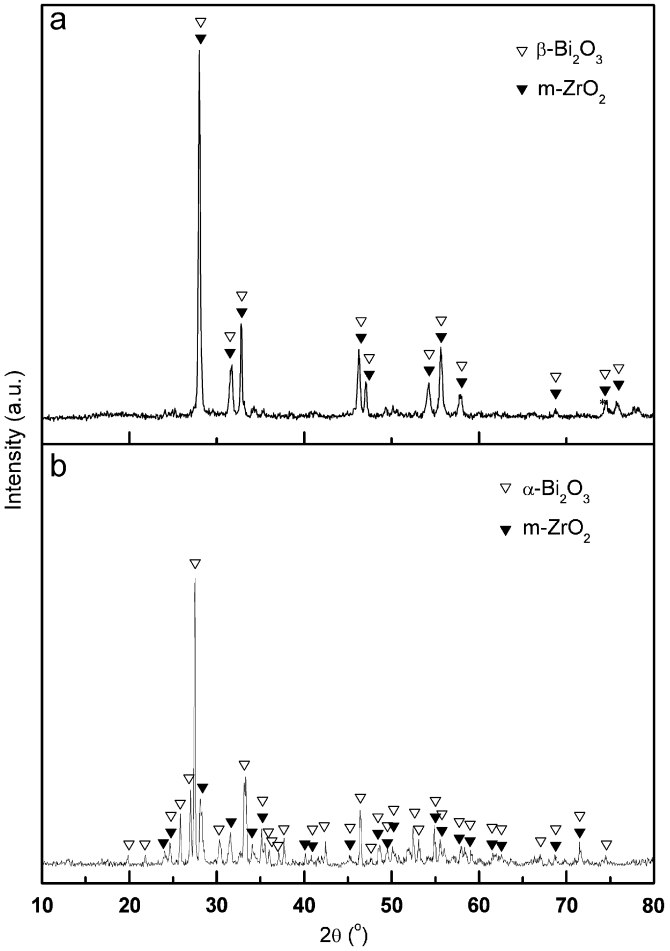


**Fig. 3.** XPD patterns of the $2Bi_2O_3 \cdot 3ZrO_2$ powder mixture mechanochemically treated for 10 h, sintered at 820 °C for 24 h and (a) quenched or (b) slowly (furnace) cooled to room temperature.

Shuk (729 °C and $\Delta_m H = 29.6\,kJ\,mol^{-1}$) [1]. According to Levin and Roth [10], the peak at 854 °C may be assigned to the melting of $Bi_2O_3$, while the small peak at 824 °C was not identified.

The sintered and quenched sample, on the first heating displays two endothermic heat effects up to 800 °C: at 634 and 705 °C (Fig. 4b). The DSC curve of this sample is similar to the curve obtained by Abrahams et al. for the $Bi_{1.85}Zr_{0.15}O_{3.075}$ phase; the positions of these peaks almost coincide with previously reported values (642 and 714 °C) [13]. Accordingly, the peak at the lower temperature may be attributed to the appearance of the $\gamma$-$Bi_2O_3$ phase, while the second peak is due to the $\gamma \rightarrow \delta$ transition. However, the results of high-temperature XPD reported by Meatza et al. [14] showed that, between about 650 and 720 °C, a complex mixture containing m-$ZrO_2$ and orthorhombic $Bi_2O_{2.3}$, besides $\gamma$-$Bi_2O_3$ as a main phase, exists. Once again, the peak at 838 °C (Fig. 4b) can be attributed to the melting of the $Bi_2O_3$ phase.

On the other hand, on the DSC traces of the powder milled for 10 h (Fig. 4c), as well as for 20 and 50 h (DSC traces not given), no remarkable thermal effects can be resolved up to 800 °C. Such an observation suggests that the high-temperature $\delta$-phase was obtained by mechanochemical treatment. Hence, during the milling the very fine mixture of the constituents, i.e., $\alpha$-$Bi_2O_3$ and m-$ZrO_2$, reacted leading to the formation of a very deformed, nanocrystalline structure resembling the $\delta$-phase. It should be noted that the lack of exothermic heat effect(s) as a characteristic for the crystallization of an amorphous, for example $Bi_4Ti_3O_{12}$ phase [26], reveals that the material is predominantly in the nanocrystalline form. These findings resolve the ambiguity in the interpretation of the foregoing XRD and TEM results.

On cooling down to 400 °C, all the samples exhibited an exothermic effect at about 570 °C, which could be attributed to the $\delta$- to $\beta$-$Bi_2O_3$ transition, while on the subsequent second heating, an endothermic heat effect appeared at around 640 °C, which plausibly arose from the opposite $\beta \rightarrow \delta$ transition.

Therefore, it seems that the reactive sintering at 820 °C (or heating up to 780 °C) produced a high-temperature-doped $\delta$-$Bi_2O_3$ phase with the nominal formula $Bi_{1.14}Zr_{0.86}O_{3+\delta}$. This phase could not be retained on cooling to room temperature, but transformed to a mixture of $\beta$-$Bi_2O_3$ and m-$ZrO_2$ at approximately 570 °C.

### 3.3. Dielectric and ferroelectric characteristics

The dielectric permittivity at room temperature of the samples prepared by reactive sintering did not depend on the employed

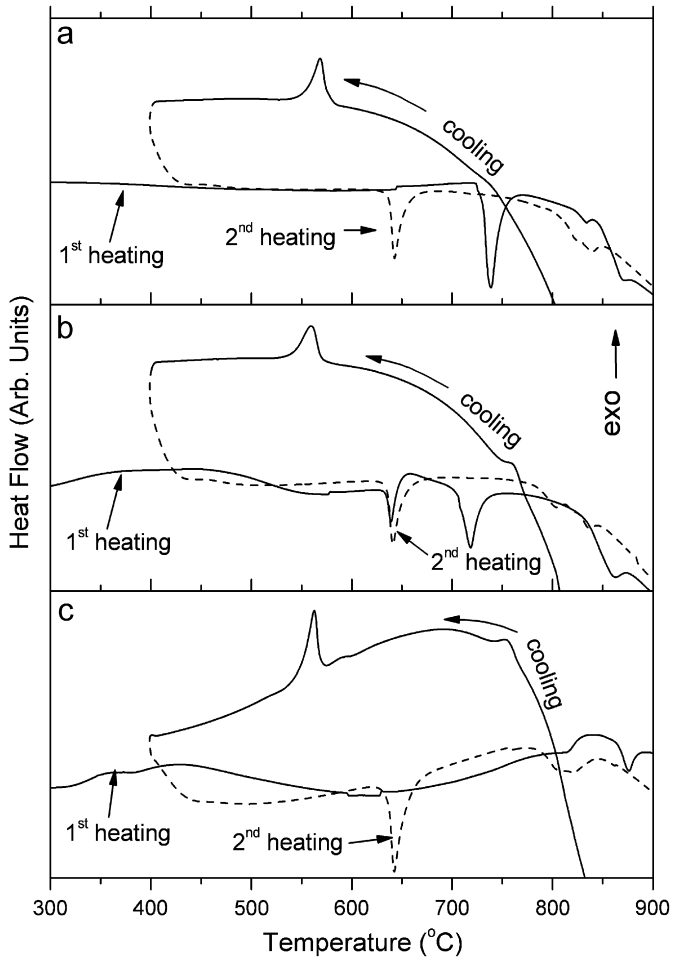


**Fig. 4.** DSC curves of the $2Bi_2O_3 \cdot 3ZrO_2$ powder mixtures: (a) before mechanochemical treatment, (b) sintered at 820 °C for 24 h and quenched, and (c) mechanochemically treated for 10 h.

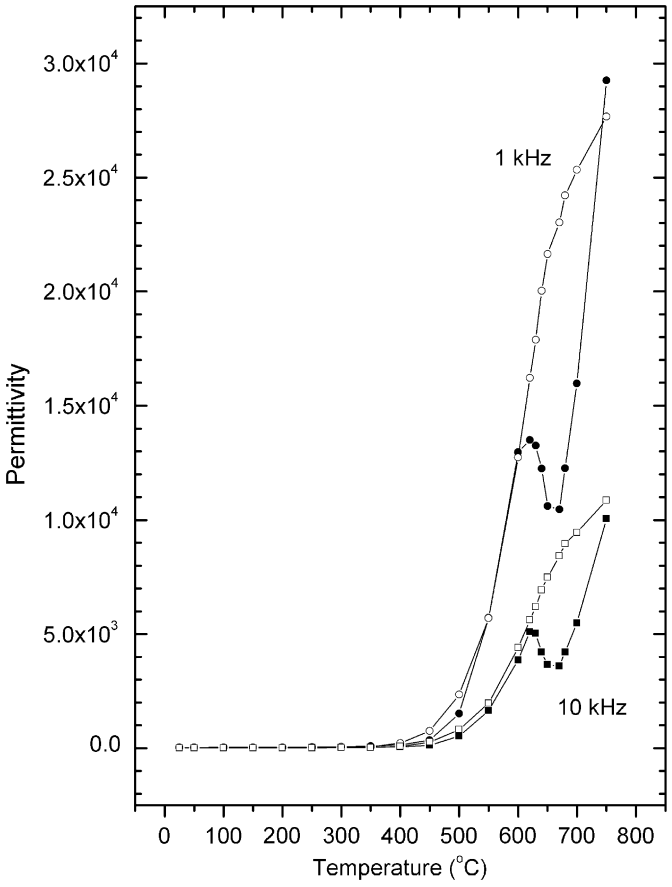


**Fig. 5.** Relative dielectric permittivity as a function of temperature for the $2Bi_2O_3 \cdot 3ZrO_2$ powder mixture mechanochemically treated for 20 h, sintered at 820 °C for 24 h and quenched (● ■) or slowly cooled (○ □) to room temperature. Circles: at 1 kHz, squares: at 10 kHz.

precursor, i.e., powders mechanochemically treated for various milling times. Thus, for the sintered and quenched samples obtained from the powders milled for 10 min to 50 h, the permittivity values were in a narrow range from 28.3 to 29.1. Such an observation is in agreement with the fact that the density of the sintered samples also did not depend on the milling time.

On the other hand, the permittivity at room temperature depends on the manner of sintering, and was around 28.5 and 11.2 for the quenched and slowly cooled samples, respectively, implying that the different values of the permittivity arise mainly from the different phase composition.

The permittivity of either the quenched or slowly cooled samples showed pronounced temperature dependence in the range 400–750 °C (Fig. 5). For example, for a quenched sample, the value of about 28 at room temperature increased to about 215 at 400 °C, and to about $1.6 \times 10^4$ at 700 °C at a frequency of 1 kHz.

As expected, the dielectric permittivity decreases with a frequency increase, but both results (at 1 and 10 kHz) confirm the existance of phase transition at the same temperature.

The anomalous behavior of the quenched samples at temperatures between 620 and 660 °C should be due to the ferroelectric to paraelectric phase transition, as a characteristic of ferroelectric materials (Fig. 5). Therefore, the peak at ~620 °C may be assigned to the Curie temperature, and is related to the transition of $\beta$- to $\delta$-$Bi_2O_3$ structural type, which, according to the DSC results, occurs at ~640 °C. The value of the dielectric permittivity at the Curie point is $1.35 \times 10^4$ at a frequency of 1 kHz. In comparison, for the $Bi_4Ti_3O_{12}$ ($2Bi_2O_3 \cdot 3TiO_2$) compound, the value of dielectric permittivity, $\varepsilon$ higher than $3 \times 10^4$ (along the *a*-axis) for the temperature above 550 °C has been reported [27] and also, $\varepsilon$ higher than $2 \times 10^4$ (measured at frequency of 1 kHz for the same temperature range) was obtained for polycrystalline $Bi_4Ti_3O_{12}$ ceramics [28].

Fig. 6 represents a typical ferroelectric (*P*–*E*) hysteresis loop, characteristic for the products obtained by reactive sintering and quenching. The values of the spontaneous, $P_s$, and remnant, $P_r$, polarization, as well as a coercive field, $E_c$, are $P_s = 17.4\,\mu C\,cm^{-2}$, $P_r = 9.2\,\mu C\,cm^{-2}$, and $E_c = 1.35\,kV\,cm^{-1}$. Both, the hysteresis dependence of the dielectric shift in an alternate electric field and the temperature dependence of the permittivity, indicate the ferroelectric nature of the quenched products. Since the m-$ZrO_2$ polymorph belongs to the centrosymmetric space group $P2_1/c$, the ferroelectricity must arise from the Bi-containing phase. This indicated the necessity for detailed structural investigations of the quenched samples.

### 3.4. Structural characterization of quenched samples

There are two main difficulties in phase and structural characterization of products obtained in the $Bi_2O_3$–$ZrO_2$ system. First, the maxima of m-$ZrO_2$ phase are hardly visible in XPD patterns when $\beta$-$Bi_2O_3$ is the major phase in the sample. This was already noticed by Levin and Roth [10] for the $6Bi_2O_3 \cdot ZrO_2$ composition (14.3 mol% of m-$ZrO_2$), and confirmed by Abrahams

et al. [13], who also could not detect m-$ZrO_2$ by the X-ray analysis, but only in the neutron powder diffraction pattern of $Bi_{1.85}Zr_{0.15}O_{3.075}$.

Hence, XPD data cannot be regarded as being suitable for thorough studies of the $\beta$-$Bi_2O_3$–m-$ZrO_2$ system. Our refinements using XPD data and the Abrahams model, in the absence or presence of m-$ZrO_2$, confirmed this conclusion. If the presence of m-$ZrO_2$ is neglected, the values of the $R_p$ and $R_{wp}$-factors were only 1–2% higher than if a mixture of $Bi_{1.85}Zr_{0.15}O_{3.075}$ and m-$ZrO_2$ was assumed. Although the differences should be judged as significant for $R_p$ values in the range 6.3–7.7% they are not very indicative for an incorrect structural model. Therefore, in the following analysis and discussion, focus will be directed toward neutron diffraction data only.

The second problem is the correct choice of the space group for doped $\beta$-$Bi_2O_3$. As stated above, the centrosymmetric space group $P4_2/nmc$ applied in previous studies during the refinement of $Bi_{1.85}Zr_{0.15}O_{3.075}$ and $Bi_{1.33}Zr_{0.67}O_{3+\delta}$ [13,14] evidently cannot be used for the present ferroelectric material, although the refinement using this space group and the Abrahams model also resulted in fairly low $R$-factors (Table 1). In such a case, the most logical choice is the space group $P\bar{4}2_1c$, as a subgroup of $P4_2/nmc$ and a widely accepted space group for pure and doped $\beta$-$Bi_2O_3$ phases (Refs. [23,25,29,30] and JCPDS card 43-0445). The calculated powder diffraction patterns in various space groups using the Abrahams model showed that the above-mentioned groups are practically indistinguishable, as several extra reflections, which should be present in the $P\bar{4}2_1c$ pattern are of zero or extremely low intensity. The present Rietveld refinement in the space group $P\bar{4}2_1c$ converged to slightly higher $R$-factors than in

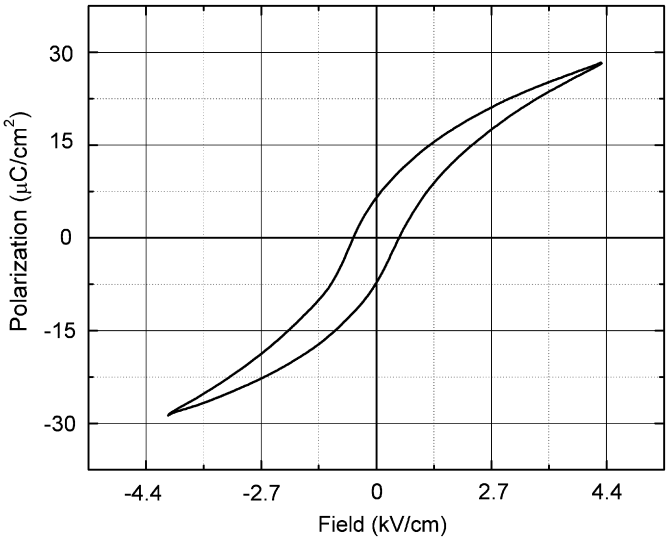


**Fig. 6.** Hysteresis loop of the $2Bi_2O_3 \cdot 3ZrO_2$ powder mixture mechanochemically treated for 20 h, sintered at 820 °C for 24 h and quenched to room temperature.

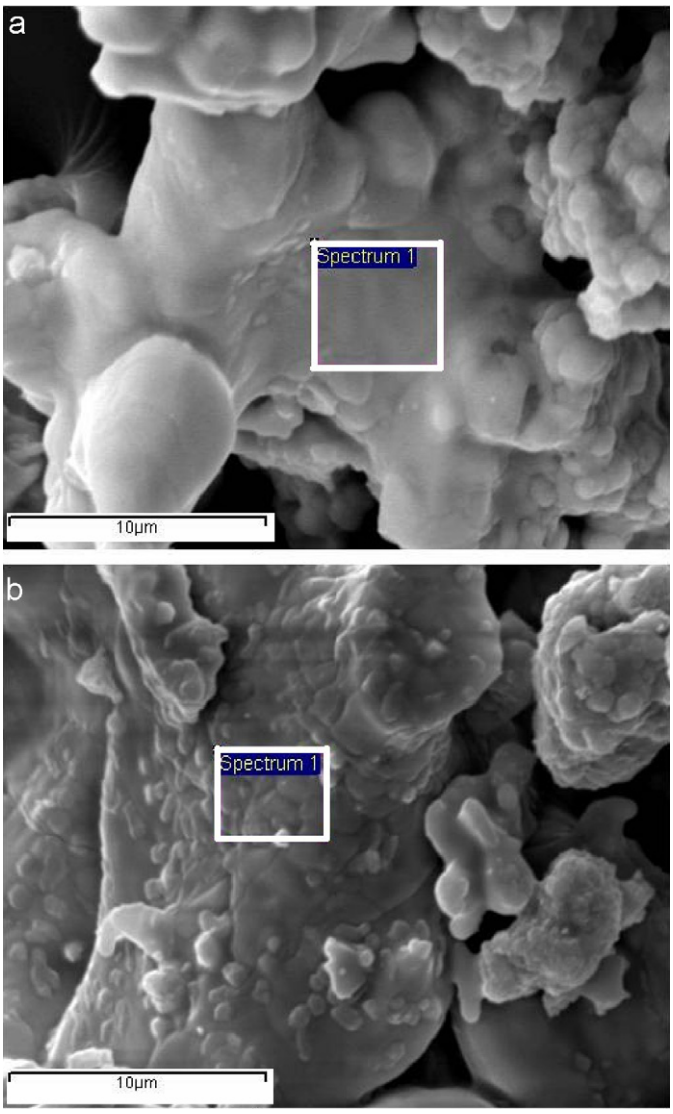


**Fig. 7.** Typical SEM micrographs of the $2Bi_2O_3 \cdot 3ZrO_2$ powder mixture heated up to 780 °C and quenched. White rectangles indicate the analyzed areas.

**Table 1**
Final results of Rietveld refinements using different structural models for the $\beta$-$Bi_2O_3$ phase and neutron diffraction data collected at 295 and 10 K

| $T$ (K) | Unit cell parameters, $a$, $c$ (Å), and unit cell volume, $V$ (Å$^3$), of $\beta$-$Bi_2O_3$ | Global $R$-factors (%) | Phase $R$-factors $\beta$-$Bi_2O_3$ $ZrO_2$ (%) | $\beta$-$Bi_2O_3$:$ZrO_2$ weight ratio (%) |
|---|---|---|---|---|
| *Abrahams model for $Bi_{1.85}Zr_{0.15}O_{3.075}$ in space group $P4_2/nmc$* | | | | |
| 295 | 7.7402(6), 5.6450(6), 338.20(5) | $R_p = 3.34$, $R_{wp} = 4.36$, $R_{exp} = 3.08$, $\chi^2 = 2.01$ | $R_B = 4.00$, $R_F = 2.14$<br>$R_B = 3.56$, $R_F = 2.06$ | 70.0(7):30.0(3) |
| *Abrahams model for $Bi_{1.85}Zr_{0.15}O_{3.075}$ in space group $P\bar{4}2_1c$* | | | | |
| 295 | 7.7400(6), 5.6445(6), 338.15(5) | $R_p = 3.51$, $R_{wp} = 4.55$, $R_{exp} = 3.07$, $\chi^2 = 2.19$ | $R_B = 4.78$, $R_F = 3.30$<br>$R_B = 4.02$, $R_F = 2.42$ | 71.5(8):28.5(3) |
| *$\beta$-$Bi_2O_3$ in space group $P\bar{4}2_1c$* | | | | |
| 295 | 7.7400(6), 5.6446(6), 338.16(5) | $R_p = 3.26$, $R_{wp} = 4.22$, $R_{exp} = 3.07$, $\chi^2 = 1.89$ | $R_B = 3.46$, $R_F = 2.01$<br>$R_B = 2.95$, $R_F = 1.51$ | 72.0(2):28.0(1) |
| 10 | 7.7346(5), 5.6198(6), 336.20(5) | $R_p = 3.52$, $R_{wp} = 4.46$, $R_{exp} = 2.06$, $\chi^2 = 2.12$ | $R_B = 3.95$, $R_F = 2.09$<br>$R_B = 4.20$, $R_F = 2.44$ | 68.5(2):31.5(1) |

the space group $P4_2/nmc$ (Table 1), probably because of the absence of a symmetry center in $P\bar{4}2_1c$.

Certainly, the presence of $ZrO_2$ stabilizes the $\beta$-$Bi_2O_3$ polymorph [10–13,18], but the upper limit of $ZrO_2$ solubility is still questionable. If unjustly high $x$ values [11,14] in general formula $Bi_{2-x}Zr_xO_{3+x/2}$ are discarded because they are based on X-ray studies, $x$ of about 0.15 seems at first sight very reasonable (Refs. [12,13] and JCPDS card 43-0445). However, even this value was not confirmed because the refinement of the $Bi_{1.85}Zr_{0.15}O_{3.075}$ structure also revealed the presence of m-$ZrO_2$ as a minor phase, whereby the phase composition of the examined sample was not reported [13].

The results of scanning electron microscopy (SEM)/EDS analyses showed that it is not possible to distinguish $\beta$-$Bi_2O_3$ and m-$ZrO_2$ phases (Fig. 7). Instead, grains larger than 10 μm without any defined shape in combination with agglomerates of submicrometer dimensions were observed. This, very likely, could be ascribed to the quenching as a step in the sample preparation. The Zr distribution, as obtained by the EDS analysis (Table 2), was not uniform and the Zr content varied over a wide range from 0.0 to 20.7 wt% (calculated for $2Bi_2O_3 \cdot 3ZrO_2$: 21.0 wt%). Nevertheless, many regions with zero or low Zr content exist.

The Rietveld refinements of the room temperature neutron diffraction data, no matter which model was assumed, consistently yielded an m-$ZrO_2$ content in the narrow range of 28.0–30.0 wt% (Table 1). These values are very close to the composition of the initial $2Bi_2O_3 \cdot 3ZrO_2$ mixture (28.4 wt%). As a minor amount of debris from the vial and ball could also be expected, the m-$ZrO_2$ content in doped $\beta$-$Bi_2O_3$ cannot exceed few weight percents. This is in agreement with the results of Ayala et al. [31], who reported that the content of Hf, as a Zr analog, in Hf-doped $\beta$-$Bi_2O_3$ cannot exceed 5 at%.

**Table 2**
Zr content as obtained by EDS analysis of the sample prepared by continuous heating up to 780 °C (heating rate: 20 °C min$^{-1}$) and quenching of the initial $2Bi_2O_3 \cdot 3ZrO_2$ powder mixture

| Point | 1 | 2 | 3 | 4 | 5 | 6 | 7 | 8 |
|---|---|---|---|---|---|---|---|---|
| Zr content (wt%) | 0.0 | 2.2(6) | 20.7(16) | 0.0 | 9.8(13) | 7.2(6) | 0.0 | 0.0 |

Estimated standard deviations are given in parentheses.

A comparison of the refined unit cell parameters listed in Table 1, which are very close to the values reported for pure $\beta$-$Bi_2O_3$ phase [23,25,29,30], also supports the previous conclusion. Since, contrary to some preceding studies [13,14], a decrease of the unit cell volume was not noticed, it was decided to finish the refinement assuming the presence of only $\beta$-$Bi_2O_3$ and m-$ZrO_2$. The lowest $R$-factors (Table 1) and the excellent agreement between the experimental and calculated diffraction profile (Fig. 8) justified this approach. The final $\Delta F$ maps also did not indicate any possible positions of Zr and additional O atom(s).

The refined atomic coordinates, displacement parameters, and selected bond distances and angles for $\beta$-$Bi_2O_3$ and m-$ZrO_2$ at 295 K are listed in the Supplementary material. A comparison of the Bi–O bond distances is given in Table 3. In $\beta$-$Bi_2O_3$, the Bi atoms are surrounded by six O atoms, three at shorter and three at longer distances. All O atoms are located in one hemisphere leaving space for the stereochemically active $Bi^{3+}$ lone electron pair. Taking into account the spread of the overall (columns) and corresponding (rows) Bi–O distances, it is not easy to compare these values. It is obvious that for the first two refinements of $\beta$-$Bi_2O_3$ (columns 1 and 2 in Table 3), the average Bi–O distances are significantly longer in comparison to the corresponding values found in the other six refinements, which, on the other hand, are similar to each other.

The Bi polyhedra are connected in such a way that channels parallel to the $c$-axis, with an approximate diameter (Bi–Bi distance) of 4 Å and an octagonal cross-section, are formed (Fig. 9). These cross-sections are irregular in cases a and b, and slightly less irregular in case c. However, they are much more regular in cases d and e, in which the entire structures look less distorted. (In fact, the structure e can be regarded as an average of the structure d.) This observation could give a possible explanation as to why the $\beta$-$Bi_2O_3$ phase is readily stabilized by the addition of $ZrO_2$, i.e., a more ordered structure is obtained. In addition, the similarity of the structures d and e can be understand as an indirect proof that the $\beta$-$Bi_2O_3$ analyzed in this study also contained some amount of Zr, although it was not detected during the structure refinement.

The refinement of the low-temperature neutron powder diffraction data (10 K) assuming a mixture of $\beta$-$Bi_2O_3$ and m-$ZrO_2$ converged to slightly higher $R$-factors in comparison to the room temperature data (Table 1). In general, the structural features, including the phase composition, were very similar to

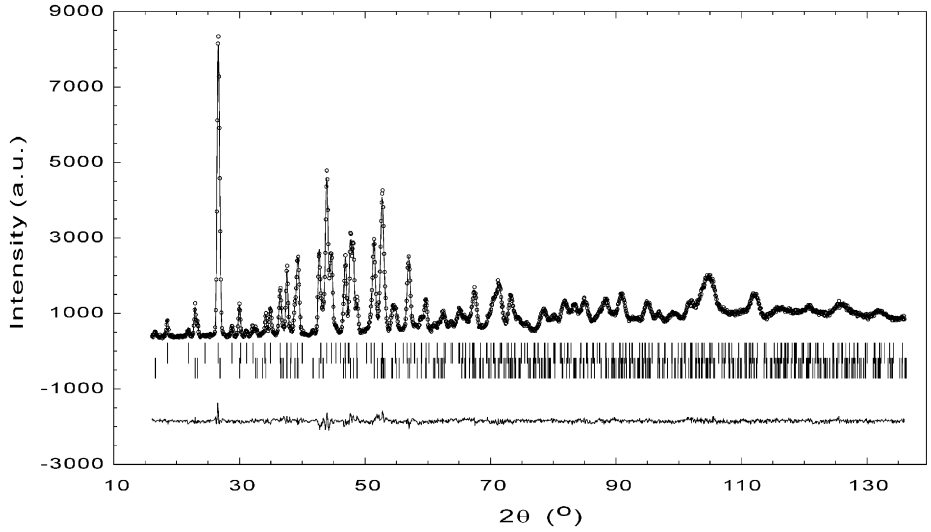


**Fig. 8.** Observed (circles), calculated (line) and difference (the lowest line) neutron powder diffraction pattern for the mixture of $\beta$-$Bi_2O_3$ and m-$ZrO_2$ at 295 K. Markers indicate reflection positions for $\beta$-$Bi_2O_3$ (top) and m-$ZrO_2$ (bottom) phase.

**Table 3**
Comparison of the Bi– O bond distances in the $BiO_6$-polyhedra for different structural models of pure and doped $\beta$-$Bi_2O_3$ phase, with the average ⟨Bi–O⟩ distances added in bold

| Literature data | | | | | This study | | |
|---|---|---|---|---|---|---|---|
| Bond | Harwig [25] | Aurivillius and Malmros [30] | Blower and Greaves [23] | Blower and Greaves, revised model [23] | Abrahams model [13] (sp. gr. $P4_2/nmc$) | Abrahams model (sp. gr. $P\bar{4}2_1c$) | The mixture of $\beta$-$Bi_2O_3$ (sp. gr. $P\bar{4}2_1c$) and m-$ZrO_2$ |
| Bi–O1 | 1.96(3) | 2.196[a] | 2.087(11) | 2.096(4) | 2.086(5)[b] [2.105(1)] | 2.093(6) | 2.097(5) |
| Bi–O2 | 2.12(6) | 2.080 | 2.094(7) | 2.128(5) | 2.185(8) [2.152(2)] | 2.159(11) | 2.157(9) |
| Bi–O2 | 2.31(6) | 2.305 | 2.176(11) | 2.253(6) | 2.199(8) [2.192(2)] | 2.246(10) | 2.236(8) |
| Bi–O2 | 2.45(6) | 2.445 | 2.530(11) | 2.463(6) | 2.541(7) [2.576(2)] | 2.595(11) | 2.593(9) |
| Bi–O1 | 3.04(9) | 2.987 | 2.736(10) | 2.720(5) | 2.713(6) [2.720(2)] | 2.697(7) | 2.687(6) |
| Bi–O2 | 3.06(9) | 3.038 | 2.988(11) | 2.977(6) | 2.886(8) [2.863(2)] | 2.798(11) | 2.817(9) |
| **⟨Bi–O⟩** | **2.49** | **2.509** | **2.435** | **2.440** | **2.435 [2.435]** | **2.431** | **2.431** |

[a] Standard uncertainties not given.
[b] The values listed in brackets are from the original literature [13].

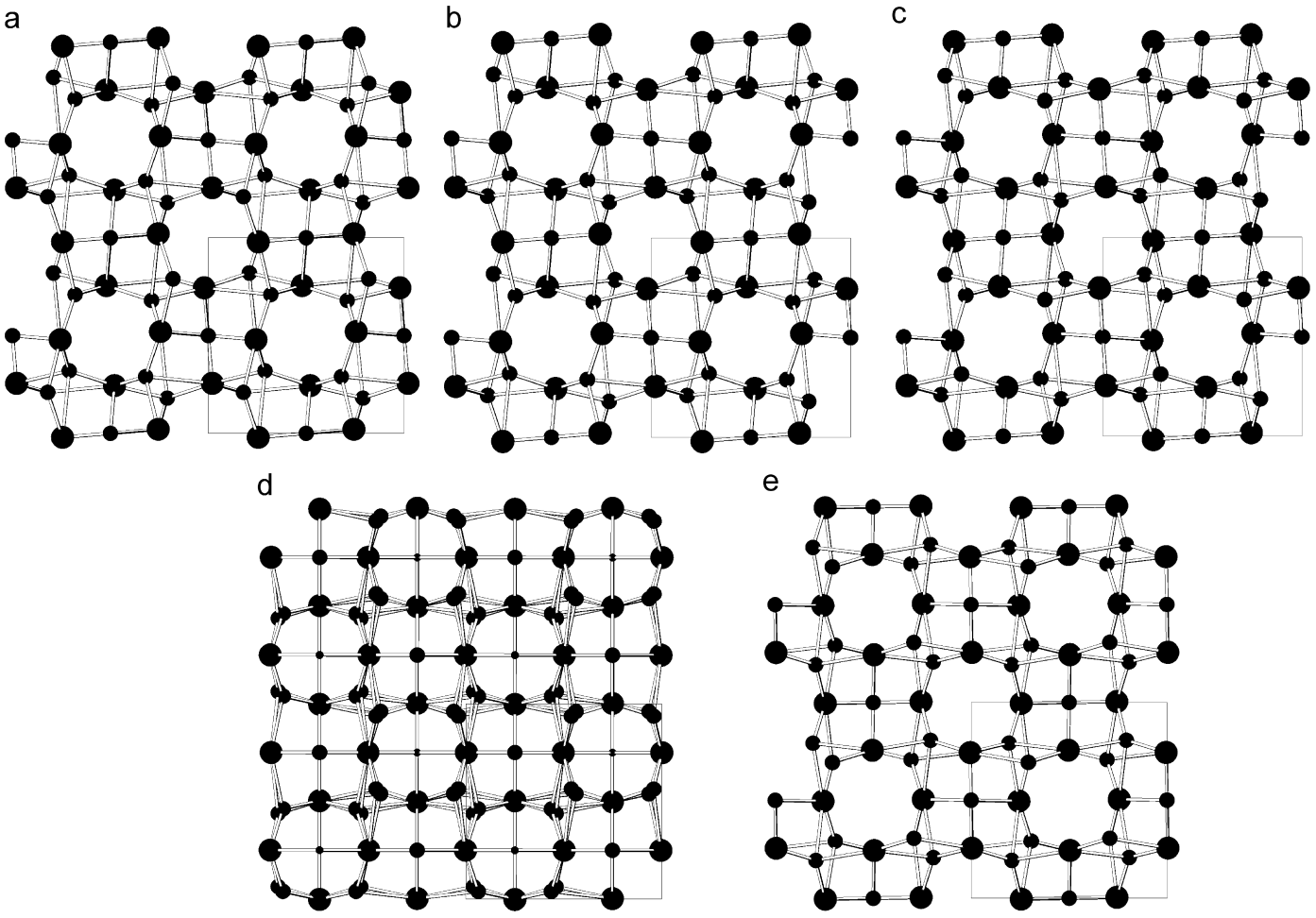


**Fig. 9.** The structures of $\beta$-$Bi_2O_3$ projected along the *c*-axis (*a*-axis down, *b*-axis right, large circles: Bi, small circles: O atoms) according to (a) Harwig, (b) Aurivillius and Malmros, (c) Blower and Greaves, revised model, (d) Abrahams et al. (the smallest circles show the positions of an additional O3 atom with 0.075 occupancy; see Section 1) and (e) this study. (For the list of references see Table 3.)

the model described above. Only expected decrease of the atomic displacement parameters, the unit cell volume and some standard uncertainties were observed for the $\beta$-$Bi_2O_3$ phase, but no systematic trends in the Bi–O bond lengths were noticed. These results also showed that $\beta$-$Bi_2O_3$ and m-$ZrO_2$ are stable below room temperature and no phase transitions occur down to 10 K.

The overall structural characteristics of m-$ZrO_2$ phase, regardless of the refinement procedure applied, are in close proximity with previous reports [32–34], and will not be discussed in detail. It is worth noticing that the refined lattice parameters and unit cell volume of m-$ZrO_2$ did not indicate the presence of Bi. This is in accordance with the observation of Sorokina and Sleight [12], who also did not detect any significant solubility of $Bi_2O_3$ in $ZrO_2$.

## 4. Conclusion

The results of a structural, thermal and electrical study of the $Bi_2O_3$–$ZrO_2$ system containing 60 mol% of $ZrO_2$ can be summarized as follows.

Mechanochemical treatment (up to 50 h) of $2Bi_2O_3 \cdot 3ZrO_2$ led to the gradual formation of a very fine nanocrystalline phase, which resembled the high-temperature $\delta$-$Bi_2O_3$ polymorph.

When mechanochemically treated samples were heated at 820 °C and slowly (furnace) cooled, complete separation to the initial $\alpha$-$Bi_2O_3$ and m-$ZrO_2$ phases was observed, i.e., $\delta$-$Bi_2O_3$ cannot be retained to room temperature by addition of $ZrO_2$.

After quenching, the mechanochemically treated and reactive sintered samples contained a mixture of $\beta$-$Bi_2O_3$ and m-$ZrO_2$ phase, confirming that $ZrO_2$ stabilizes the $\beta$-$Bi_2O_3$ polymorph.

The relative dielectric permittivity of both the quenched or slowly cooled samples showed pronounced temperature dependence, but the quenched samples, in addition, possessed ferroelectric properties with a Curie temperature at about 620 °C. Because m-$ZrO_2$ crystallizes in a centrosymmetric space group, the ferroelectricity must be related to the presence of $ZrO_2$-doped $\beta$-$Bi_2O_3$ phase. To the best of our knowledge, the ferroelectricity of $\beta$-$Bi_2O_3$ phase has not been reported before.

The Rietveld refinement of the $\beta$-$Bi_2O_3$/m-$ZrO_2$ mixture using neutron powder diffraction data collected at 295 and 10 K confirmed the non-centrosymetric space group $P\bar{4}2_1c$ as the true space group for $ZrO_2$-doped $\beta$-$Bi_2O_3$. The $ZrO_2$ content in the $\beta$-$Bi_2O_3$/m-$ZrO_2$ mixture, as obtained by the Rietveld analysis (28.0–30.0 wt%), is very close to the composition of the initial $2Bi_2O_3 \cdot 3ZrO_2$ mixture (28.4 wt%). This means that the $ZrO_2$ percentage in doped $\beta$-$Bi_2O_3$ phase must be very low, which is opposed to the results of most previous studies.

## Acknowledgments

This work was financially supported by the Ministry of Science of Republic of Serbia, Grants no. 142030 and 141027. The authors wish to thank Prof. Roland Tellgren, Ångsrom Laboratory, Uppsala University, Uppsala, Sweden, for the neutron diffraction measurements, and Prof. Nataša Bibić, Institute for Nuclear Sciences "Vinča", Belgrade, Serbia, for performing the TEM analysis.

## Appendix A. Supplementary material

Supplementary data associated with this article can be found in the online version at doi:10.1016/j.jssc.2008.02.038.

Further details of the crystal structure investigation(s) can be obtained from the Fachinformationszentrum Karlsruhe, 76344 Eggenstein-Leopoldshafen, Germany (fax: +49 7247 808 666; e-mail: crysdata@fiz.karlsruhe.de) on quoting the depository numbers CSD417638 ($\beta$-$Bi_2O_3$) and CSD417639 ($ZrO_2$).

## References

[1] P. Shuk, H.D. Wiemhofer, U. Guth, W. Gopel, M. Greenblatt, Solid State Ionics 89 (1996) 179–196.
[2] J.C. Boivin, G. Mairesse, Chem. Mater. 10 (1998) 2870–2888.
[3] A.R. West, Basic Solid State Chemistry, second ed, Wiley, Chichester, 2004, pp. 345−346.
[4] J.H. Kim, G.M. Choi, Solid State Ionics 130 (2000) 157–168.
[5] K. Sasaki, J. Maier, Solid State Ionics 134 (2000) 303–321.
[6] S.C. Singhal, Ceram. Bull. 82 (2003) 9601–9610.
[7] H. Ishiwara, M. Okuyama, Y. Arimoto (Eds.), Ferroelectric Random Access Memories—Fundamentals and Applications (Topics in Applied Physics), vol. 93, Springer, Berlin, Heidelberg, 2004.
[8] Č. Jovalekić, B. Stojanović, M. Zdujić, M. Mitić, J. Mater. Sci.: Mater. Electron. 15 (2004) 499–504.
[9] B. Aurivillius, L.G. Sillen, Nature 155 (1945) 305–306.
[10] E.M. Levin, R.S. Roth, J. Res. Natl. Bur. Stand. A: Phys. Chem. 68A (1968) 197–206.
[11] F. Hund, Z. Anorg. Allg. Chem. 333 (1964) 248–255.
[12] S.L. Sorokina, A.W. Sleight, Mater. Res. Bull. 33 (1998) 1077–1081.
[13] I. Abrahams, A.J. Bush, S.C.M. Chan, F. Krok, W. Wrobel, J. Mater. Chem. 11 (2001) 1715–1721.
[14] I. De Meatza, J.P. Chapman, F. Mauvy, J.I. De Larramendi, M.I. Arriortua, T. Rojo, Mater. Res. Bull. 39 (2004) 1841–1847.
[15] A.R. Yavari, Mater. Trans. JIM 36 (1995) 228–239.
[16] E. Gaffet, G. Le Caër, in: H.S. Nalwa (Ed.), Encyclopedia of Nanoscience and Nanotechnology, vol. 10, American Scientific Publishers, Stevenson Ranch, California, 2004, pp. 1–39.
[17] M. Zdujić, in: A.M. Spasic, Jyh-Ping Hsu (Eds.), Finely Dispersed Particles: Micro-, Nano-, and Atto-Engineering, Taylor & Francis, Boca Raton, 2006, pp. 435–461.
[18] D. Poleti, Lj. Karanović, M. Zdujić, Č. Jovalekić, Z. Branković, Solid State Sci. 6 (2004) 239–245.
[19] S.K. Pradhan, H. Dutta, Physica E 27 (2005) 405–419.
[20] W. Kraus, G. Nolze, PowderCell for Windows, V2.4, Federal Institute for Materials Research and Testing, Berlin, Germany.
[21] J. Rodrigez-Carvajal, FULLPROF: A Program for Rietveld Refinement and Pattern Matching Analysis, Abstracts of the Satellite Meeting on Powder Diffraction of the XV Congress of the IUCr, Toulouse, France, 1990, p. 127.
[22] T. Roisnel, J. Rodrigez-Carvajal, Mater. Sci. Forum 378–391 (2001) 118–123.
[23] S.K. Blower, C. Greaves, Acta Crystallogr. C 44 (1988) 587–589.
[24] M. Winterer, R. Delaplane, R. McGreevy, J. Appl. Crystallogr. 35 (2002) 434–442.
[25] H.A. Harwig, Z. Anorg. Allg. Chem. 444 (1978) 151–166.
[26] M. Zdujić, D. Poleti, Č. Jovalekić, Lj. Karanović, J. Non-Cryst. Solids 352 (2006) 3058–3065.
[27] A. Fouskova, L.E. Cross, J. Appl. Phys. 41 (1970) 2834–2838.
[28] V.A. Podolskii, E.F. Dudnik, T.M. Stolpakova, Izv. Akad. Nauk. SSSR Ser. Fiz. 39 (1975) 1041–1043 (in Russian).
[29] G. Gattow, D. Schütze, Z. Anorg. Allg. Chem. 328 (1964) 44–68.
[30] B. Aurivillius, G. Malmros, K. Tekn. Högsk. Handl. 291 (1972) 545–562.
[31] A. Ayala, A. López-Garcia, A.G. Leyva, M.A.R. De Benyacar, Solid State Commun. 99 (1996) 451–455.
[32] D.K. Smith Jr., H.W. Newkirk, Acta Crystallogr. 18 (1965) 983–991.
[33] A. Gualtieri, P. Norby, J. Hanson, J. Hriljac, J. Appl. Crystallogr. 29 (1996) 707–713.
[34] M. Winterer, R. Delaplane, R. McGreevy, J. Appl. Crystallogr. 35 (2002) 434–442.